Spin-polarized photoemission spectroscopy of magnetic surfaces using undulator radiation

P. D. Johnson and N. B. Brookes
Physics Department, Brookhaven National Laboratory, Upton, New York 11973

S. L. Hulbert and R. Klaffky
National Synchrotron Light Source, Brookhaven National Laboratory, Upton, New York 11973

A. Clarke[a] and B. Sinković[b]
Physics Department, Brookhaven National Laboratory, Upton, New York 11973, and AT&T Bell Laboratories, Murray Hill, New Jersey 07974

N. V. Smith
AT&T Bell Laboratories, Murray Hill, New Jersey 07974

R. Celotta, M. H. Kelly, D. T. Pierce, M. R. Scheinfein,[c] and B. J. Waclawski
National Institute of Standards and Technology, Gaithersburg, Maryland 20899

M. R. Howells
Advanced Light Source, Lawrence Berkeley Laboratory, Berkeley, California 94720

(Received 30 August 1991; accepted for publication 23 November 1991)

A beamline has been established at the National Synchrotron Light Source to perform angle-resolved photoemission experiments on magnetic surfaces with spin sensitivity. The system has two novel features: it uses a miniature electron-spin polarization analyzer and it also uses synchrotron radiation from an undulator rather than a bending magnet.

I. INTRODUCTION

Photoemission is now well established as the primary technique in the study of the electronic structure of atoms, molecules, and solid materials. For the solid state, selection rules and the use of different light polarizations allow the determination of the symmetry of the initial state. Further, with the extension to angle-resolved photoemission,[1] both the momentum and the energy of the photoemitted electron may be determined. This allows the electronic band structure to be completely mapped. Spin analysis of the photoemitted electrons offers the possibility of more detailed studies of the electronic properties of ferromagnetic systems. In the first spin-polarized photoemission measurements the sample was magnetized perpendicular to its surface along the electron optical axis. This results in an external magnetic field and consequent loss of information on the angle of electron emission.[2] An important advance in the development of spin-polarized photoemission was the demonstration that photoemitted electrons could be measured with the sample magnetized in the sample plane, that is transverse to the electron optical axis.[3] In this geometry there is minimal penetration of the magnetic field outside the sample and angle-resolved, spin-analyzed photoemission spectra can be measured. Angle-resolved, spin-polarized photoemission has been applied to more and more systems, including the electronic structure of bulk ferromagnets,[4] adsorbate covered surfaces,[5] and ultrathin films.[6]

One limitation of spin-polarized photoemission is the inherent inefficiency of the spin detectors. The "efficiency factor" of such detectors is typically 10^{-4} resulting in acquisition times at least 10^4 times longer for a signal-to-noise ratio equivalent to the normal photoemission spectrum.[7] However, the inefficiency can be compensated for through the use of photon sources that are capable of producing extremely high fluxes; such sources are the new undulators currently being installed on a number of electron storage rings.

In this paper we describe a beamline designed to explore the use of undulator radiation for spin-polarized photoemission. We further describe in detail the experimental configuration for measuring the energy, momentum, and spin of the photoemitted electrons. The instrument has benefited from the introduction of the low-energy NIST spin detector.[8] Because of its compact size, this detector allows more flexibility in the angular measurements than the traditional Mott detector. We note in passing that the low-energy electron diffraction (LEED) detector,[9] the more recent low-energy scattering detector[10] and the very-low-energy scattering detector[11] can also be made quite compact.

II. APPARATUS

As already noted, spin detection is a relatively inefficient process but this may be compensated for through the use of more intense light sources and, in particular, in the field of synchrotron radiation, through the use of undulator-derived radiation. The present experiment was estab-

[a]Present address: Kodak Ltd., Surface Science W93, Healstone Drive, Harrow, Middlesex HA1 4OY, UK.
[b]Present address: Physics Dept., New York University, 2 Washington Place, NY, NY 10003.
[c]Present address: Dept. of Physics and Astronomy, Arizona State University, Tempe, AZ 85287.

lished to examine the use of such radiation. In the initial stage of development it was found to be convenient to use a miniaturized version of the toroidal grating monochromator (TGM) to monochromatize the radiation from the undulator. We note, however, that this particular aspect of the experiment is currently being modified. In the following sections we discuss the facility in two parts: first, those components involved in the delivery of monochromatic photons to the sample, and second, the measurement chamber incorporating sample preparation and characterization facilities together with the spin-polarized photoelectron spectrometer.

A. Photon delivery

The light for these experiments was provided by the U5U undulator on the VUV storage ring at the NSLS, Brookhaven. Since the properties of the U5U undulator have been reported in detail before,[12] they will only be outlined here.

The desirable feature of an undulator is the high photon flux available. This may typically be 250–500 times the flux emitted per mrad from a bending magnet source. Temporal coherence between wavefronts emitted along the path of an undulator leads to spectral output with characteristic harmonics of the fundamental ($n=1$) whose wavelength is given by[13]

$$\lambda(K,\vartheta)=\frac{\lambda_0}{2n\gamma^2}\left(1+\frac{K^2}{2}+\gamma^2\vartheta^2\right),\quad n=1,3,5,\ldots,\qquad(1)$$

where λ_0 is the magnetic period length (6.5 cm), γ is the storage ring energy measured in rest mass units (1456), ϑ is the observation angle with respect to the undulator axis, and K is a parameter related to the peak magnetic field strength, B_0, such that

$$K=0.934\lambda_0(\mathrm{cm})B_0(\mathrm{T}).\qquad(2)$$

For $K\sim1$ (the so-called undulator regime), the angular deflection of the electron beam in the device is comparable to the maximum angular deflection of the emitted light and the spectral output is dominated by characteristic harmonic peaks. Equation (1) is the zero emittance limit. However, it should be noted that in practice, due to the finite electron-beam emittance, even harmonics are also observed.[12]

The original VUV undulator installed on the NSLS UV ring and used in the development of the spin-polarized experiments was of the permanent magnet $SmCo_5$ type. With a period length of 6.5 cm and the minimum possible vertical gap of 39.6 mm, the spectral output, shown in Fig. 1, is characterized by the first harmonic at 56 eV photon energy. The photon energy can be tuned by adjusting the gap to alter the magnetic field which enters Eq. (1) via the parameter K or by changing the stored beam energy γ. Indeed, because of the limitations imposed by the minimum gap setting, several experiments have been successfully carried out with the first harmonic at 52 eV corresponding to $\gamma=1405$ (718 MeV). The disadvantage of this mode of tuning is that the lifetime of the VUV storage ring, which is limited by the Touschek effect, is strongly energy dependent (going approximately as γ^3).[14]

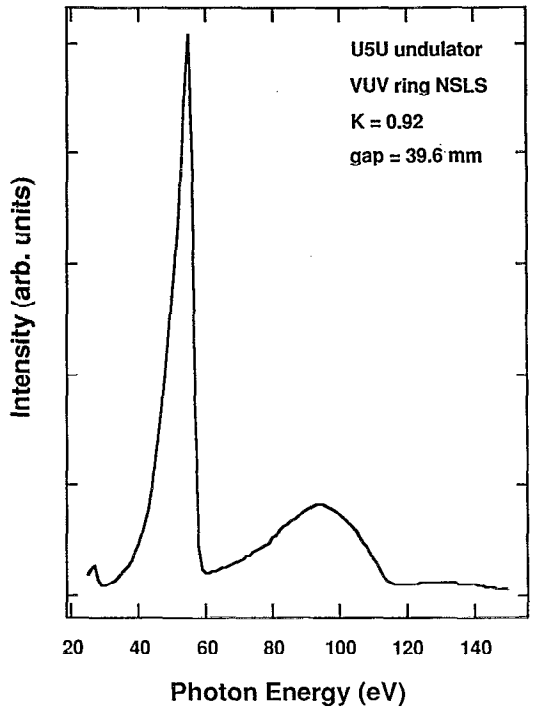

FIG. 1. Output of the U5U undulator showing the first and second harmonics.

The term in $\gamma\vartheta$ in Eq. (1) determines the angular broadening due to observation at angle ϑ to the undulator axis. On axis the linewidth of each harmonic n is given approximately by

$$\frac{\Delta\lambda_n}{\lambda_n}\approx\frac{1}{nN}\quad(n=1,3,5,\ldots),\qquad(3)$$

where N ($=38$) is the number of magnetic periods. This gives a width of about 1.5 eV with the first harmonic at 56 eV. Evidently the undulator requires some form of additional monochromatization to achieve the higher-energy resolution (<0.5 eV) needed for the photoemission experiments.

It should also be noted that the radiation is highly collimated, the half angle of emission being proportional to $(1/\gamma)(1/\sqrt{nN})$. With the first harmonic at minimum gap this is approximately 100 μrad for the U5U undulator. This particular property leads to a potentially easier task in attempting to match to the standard optics of a beamline.

Perhaps the simplest form of grazing incidence monochromator is that based on the toroidal grating. Relying on approximate focusing, such devices have the advantages of high flux, mechanical simplicity, and low cost.[15] Under certain conditions[16] the entrance arm length l_A and exit arm length l_B of a TGM may be shown to be related to the major radius R by the formula

$$R=\frac{2}{\cos\phi}\left(\frac{1}{l_A}+\frac{1}{l_B}\right)^{-1},\qquad(4)$$

where ϕ is the angle of incidence. The minor radius r and major radius are related by the formula

$$r = R \cos^2 \phi. \tag{5}$$

Thus, having selected some included angle appropriate to the desired energy range, these formulae show that l_A and l_B may be scaled to any size, with the corresponding radii R and r. However, the factors that determine the resolution place a lower limit on this process. Thus the source size limit is given by[17]

$$\Delta\lambda_s = \frac{s \cos \phi}{dml_A}, \tag{6}$$

where s is the slit size, d is the grating groove density, m is the diffraction order, and ϕ and l_A are, as before, the angle of incidence and the entrance arm length, respectively. If the ratio s/l_A is maintained constant, the aberration and slit-width-limited resolution of the system are unchanged. However, we note that the phase space acceptance of the system is reduced, pointing to the value of a source with small emittance, a requirement that puts more demands on the input optics focusing the radiation onto the entrance slit.

Based on previous TGM designs, an included angle of 150° and a ruled density of 1200 lines/mm was chosen to cover the range corresponding to the output of the undulator. For this range the entrance and exit arms have the lengths $0.22R$ and $0.3R$, respectively, where R is the major radius. Space considerations make the choice of R equal to 1 m appropriate. Figure 2 shows the calculated resolution of the monochromator.

An important consideration in the design of such a beamline is the choice of focusing element for the entrance optics. Because of the extended nature of the source it becomes necessary to use an entrance mirror with large demagnification in order to make full use of the photon flux available from the entire length of the device, i.e., to match the monochromator phase space. However, too large a demagnification results in a loss of energy resolution due to increased filling of the grating in the sagittal plane and the consequent problems relating to astigmatic coma. Some choice has to be made that minimizes these problems. Somewhat fortuitously, it was found that the parabolic mirror previously used as an exit mirror on the NSLS Plane Grating Monochromator (PGM) was well matched to these requirements. This mirror was originally designed to focus light from an infinite source point into an image 1.08 m away. Positioned 8.25 m from the undulator center, it focuses the collimated light beam into a spot approximately 1.25 m from its center, the demagnification being of the order 6.6:1.

A schematic of the beamline is shown in Fig. 3. Initially, the sample was placed ~0.2 m from the exit slits. The post-focusing mirror was a later addition as explained below. The first element of the input optics is a simple plane mirror which deflects the undulator light onto the focusing paraboloid. The plane mirror has the advantage that it is easy and inexpensive to replace if necessary.

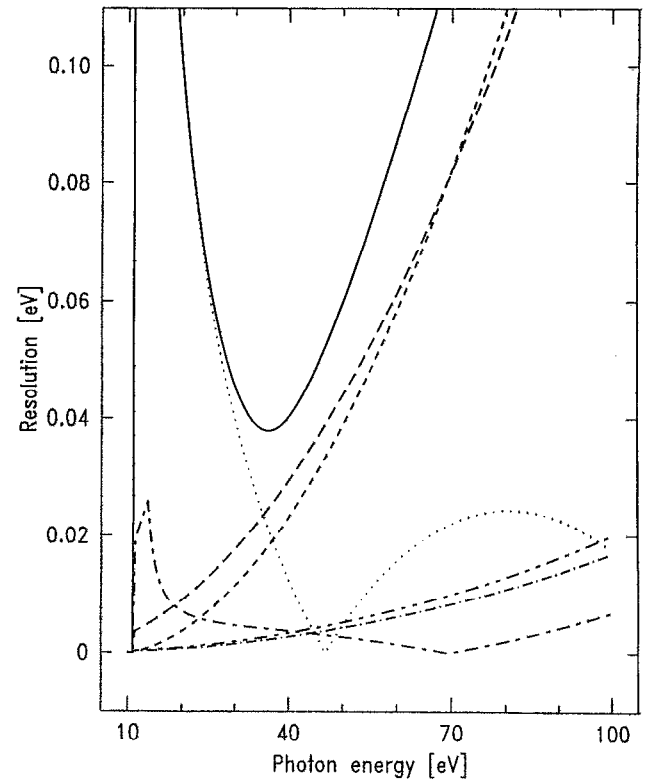

FIG. 2. Photon energy resolution of the Cricket toroidal grating monochromator vs photon energy. The total resolution (solid line) is the quadrature sum of the following contributions: 25-μm entrance slit (short dashed line), 25-μm exit slit (long dashed line), grating defocus abberation (dotted line), grating coma abberation (long-short-long dashed line), grating astigmatic coma aberration (long-short-short-long dashed line), and 1-arcsec grating figure error (dash-dotted line). The abberation terms assume 5.6 mrad (7.2 mrad) vertical (horizontal) illumination of the 25 mm×25 mm grating surface by the demagnifying paraboloidal mirror upstream of the monochromator. The 1200 line/mm grating has 1 m (61 mm) tangential (sagittal) radius and is used in a 150° constant included angle geometry with 219.6 mm (300 mm) entrance (exit) arm lengths.

Using the SHADOW ray tracing program[18] the beamline was ray traced up to the exit slits. Following standard procedures[19] in specifying the effective source size of the undulator we find that Σ_h and Σ_v, the respective rms horizontal and vertical source sizes, are given by

$$\Sigma_{h,v} = \sqrt{\sigma_{h,v}^2 + \sigma_R^2}, \tag{7a}$$

where

$$\sigma_R = (L/4\pi)\sigma'_R \tag{7b}$$

and $\sigma_{h,v}$ refers to the electron-beam sizes. σ'_R, the diffraction-limited opening angle, is given by

$$\sigma'_R \approx \frac{1}{\gamma\sqrt{2nN}}\left(1 + \frac{K^2}{2}\right)^{1/2} = \sqrt{\frac{\lambda_n}{L}}, \tag{8}$$

where L is the length of the undulator and λ_n is the wavelength of the nth harmonic. With the parameters appropriate to the NSLS VUV ring we find that Σ_h and Σ_v are 1.24 and 0.171 mm, respectively.

Figure 4 shows the calculated transmission of the beamline as a function of slit widths. The transmission is

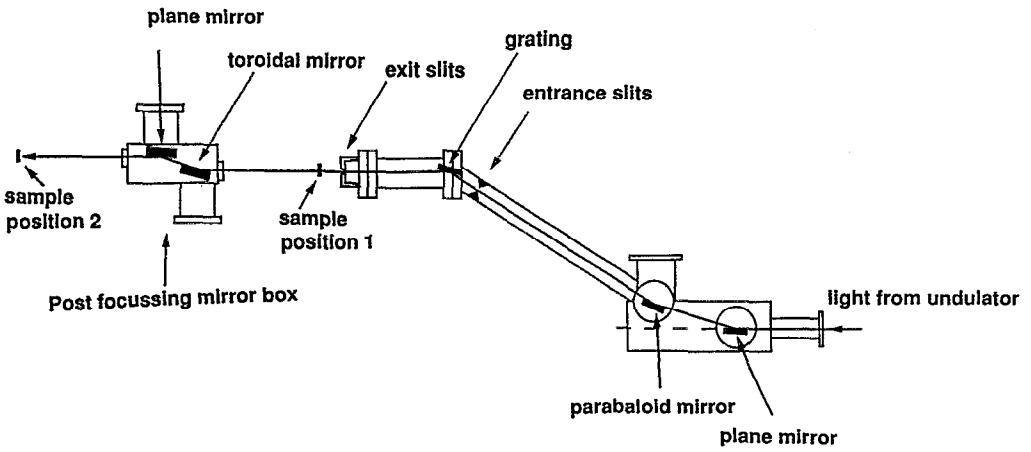

FIG. 3. A schematic diagram of the U5U beamline optical arrangement. Sample position 1 represents the arrangement in early work and is the appropriate position for the results of the calculations shown in Fig. 4. The spectra shown in Figs. 6–8 are with the sample at position 2, after post-focusing optics were installed (see text).

defined as a fraction of the flux emitted from the source with no reference to the harmonic structure of the undulator as defined by Eq. (1). From Figs. 2, 3, and 4 we see that the design of a simple beamline based on the miniaturized TGM provided the possibility of extremely high photon fluxes with relatively high resolution. With the dimensions of the instrument described here it is possible to place the target area behind the exit slits with no further focusing optics, and the initial experiments were done in this configuration. However, with such a configuration the inability to valve the monochromator off from the chamber, the exit slits being in the sample chamber, presents a considerable disadvantage for surface science studies. Thus a post-focusing mirror was incorporated into the beamline as shown in Fig. 3. This toroidal mirror focused the exit slit to a small spot at the sample with 1:1 focusing in the vertical direction. A plane mirror returns the light to the horizontal on entering the sample chamber. The loss in intensity due to the extra reflections is more than compensated for by the focusing of the light.

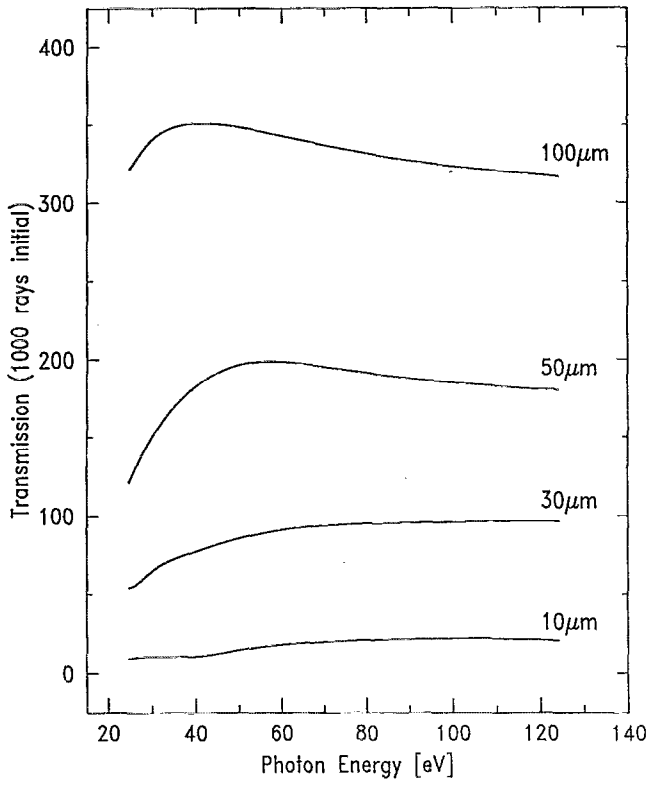

FIG. 4. Overall efficiency of the Cricket toroidal grating monochromator vs photon energy. The number of transmitted rays is shown for four values of slit openings (entrance and exit): 10, 30, 50, and 100 μm. The number of source rays is normalized to 1000 for these calculations.

B. Electron angle, energy, and spin analysis

The spin-polarized photoelectron spectrometer consists of a commercial hemispherical electron energy analyzer (50 mm mean radius)[20] mounted on a single-axis goniometer and a low-energy diffuse scattering spin analyzer. The energy analyzer, spin detector, and transport optics are shown schematically in Fig. 5(a). The initial version of the spin analyzer[8] coupled to the energy analyzer has since been replaced by a second version,[21] which is what is shown in Fig. 5(a). The size of the spin detector does not restrict the motion or angular range of the energy analyzer, in contrast to a conventional high-energy Mott detector.[22] The overall size of the present detector is $\sim$65 mm diam by $\sim$50 mm depth. We are thus able to measure spin-polarized angle-resolved photoelectron spectra over a range of incident light and photoelectron emission angles determined solely by the physical size of the energy analyzer. The angle of incidence of the light (θ_i) can be varied continuously from $\theta_i = 35°$ to grazing angles and the emission angles (θ_e) attainable are from $\theta_e = -35°$ (towards the light) to $\theta_e = 45°$, the latter angle largely determined by the sample manipulator size.

Care must be taken in coupling the electron spectrometer to the spin analyzer with minimal loss of electrons. In the present case, the original exit optics of the hemispherical energy analyzer with slight modification were adequate for transport to the spin detector. These optics are shown in Fig. 5(b). The effective lens potentials, i.e., the electron kinetic energy plus the lens voltage, are shown for an analyzer pass energy of 25 eV. The Au target is at the same potential as the last lens element. The electron-beam envelope for electrons photoemitted from the sample with a kinetic energy of 55 eV is shown for both the parallel and

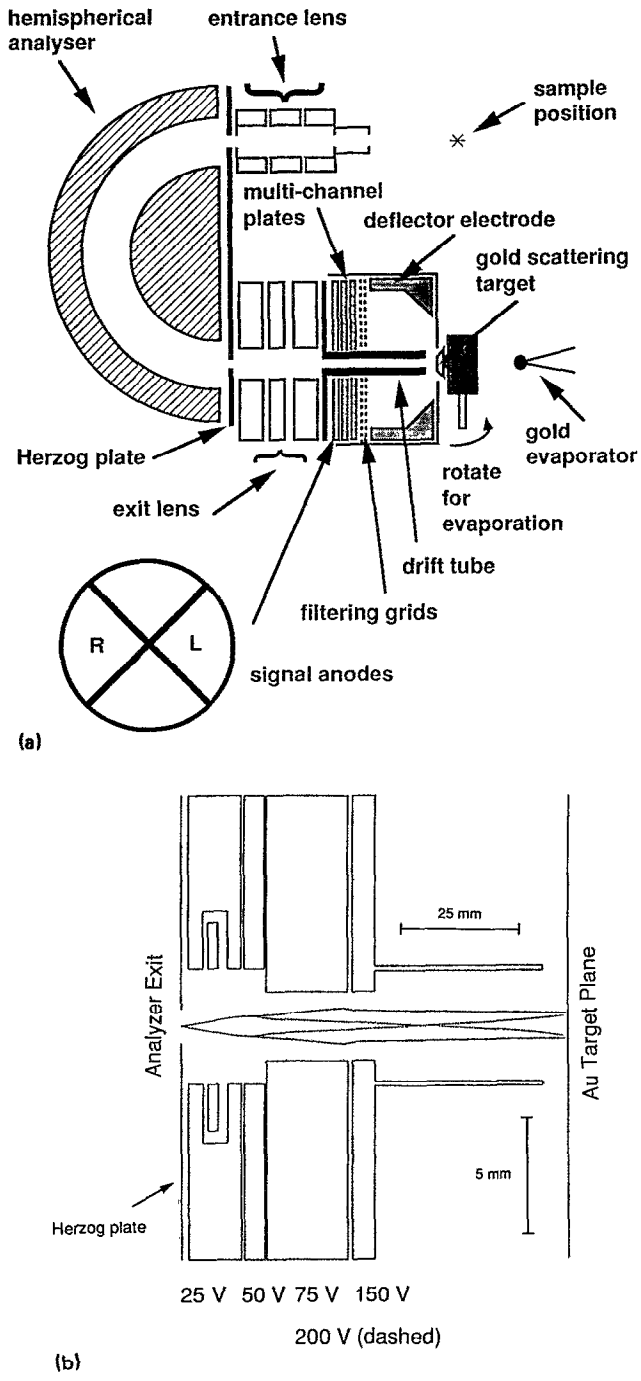

FIG. 5. (a) A schematic diagram of the hemispherical analyzer with electron transport optics and spin detector shown. (b) Electron optics to transport electrons from the energy analyzer to the Au target shown with effective lens potentials for an analyzer pass energy of 25 eV. The electron-beam envelope for 55-eV photoelectrons is shown for the parallel mode (solid line) and the compensated mode (dashed line) with two different potentials for the third lens element. Note that the vertical scale is expanded five times with respect to the horizontal scale. The distance from the energy analyzer exit aperture, in the Herzog plate, to the Au target plane is 81 mm. The first lens element contains two sets of deflector plates in the horizontal and vertical planes.

compensated modes of operation. In the compensated mode, shifts in beam position at the Au target are accompanied by angle changes such that their respective contributions to the apparatus asymmetry cancel.[21]

The spin analyzer scattering target is a polycrystalline gold film which is prepared by *in situ* evaporation. The target is rotated 180° to face a gold evaporator [Fig. 5(a)]. This allows the film to be refreshed as required, typically every few days. Electrons backscattered from the target pass through retarding grids which reject low-energy secondary electrons and transmit only those electrons that carry the spin information.[8] The deflector electrode, first grid potentials, and the geometrical arrangement of the components determine the range of angles collected and optimize the electron trajectories for efficient filtering by the grids.[21] Transmitted electrons are multiplied by multichannel plates and the resulting charge pulses are detected at one of the four quadrants of the anode assembly, Fig. 5(a). The multichannel plates are operated at a gain that allows for stable discrimination. The spin-dependent asymmetry in the scattering from the Au targets is a consequence of the spin-orbit interaction. The asymmetry is characterized by the Sherman function $S(\vartheta)$, which is averaged over a range of ϑ and for the present detector has a value $S = 0.10$.[21] The relative efficiency of spin polarimeters may be described by a figure of merit (FOM) given by $S^2 I/I_0$, where I/I_0 is a measure of the reflected intensity within the detector.[22] The FOM for this spin polarimeter is 10^{-4}, which compares well with other such devices.[8,21]

In all measurements it is crucial that the sample is put reproducibly into one of two oppositely magnetized remanent states. Multidomain systems may give irreproducible results with lower polarization. A 2-A dc current passed through a two-turn coil was sufficient to remanently magnetize the iron picture frame sample used in the measurements described here. For the case of thin magnetic films, a fast ($\sim$250-μs), high-current pulse run through a 20-turn coil placed next to the sample was used. Two measurements of the spin polarization are made, one with the sample magnetized "up" (I_L^+, I_R^+) and one with the sample magnetized "down" (I_L^-, I_R^-), where I_L (I_R) is the number of electrons scattered to the left (right), respectively, from the Au target in the spin analyzer and detected at the anodes [Fig. 5(a)]. Any instrumental asymmetry can then be removed by combining the four measurements. The true spin polarization (P) is given by[22]

$$P = \frac{1}{S} \frac{\sqrt{I_L^+ I_R^-} - \sqrt{I_L^- I_R^+}}{\sqrt{I_L^+ I_R^-} + \sqrt{I_L^- I_R^+}}, \tag{9}$$

where S is the effective Sherman function. Assuming that the incident beam does not move between "+" and "−" measurements, the measured intensities combined in this manner removes, to first order, any instrumental asymmetry derived from a misalignment of the beam incident on the scattering target. The two measurements, however, may have different count rates without affecting the measured polarization. The instrumental asymmetry (A) is given by

$$A = \frac{\sqrt{I_L^+ I_L^-}}{\sqrt{I_R^+ I_R^-}}, \tag{10}$$

assuming there is no asymmetry that changes for the two magnetization directions. However, such effects can be identified as described below.

The individual spin-up and spin-down spectra are obtained from the polarization P [Eq. (9)] by

$$I^{\uparrow} = \langle I \rangle (1+P), \quad I^{\downarrow} = \langle I \rangle (1-P), \tag{11}$$

where

$$\langle I \rangle = \frac{I_L^+ + I_L^- + I_R^+ + I_R^-}{4}. \tag{12}$$

The statistical errors in the polarization and spin intensities are calculated as

$$\delta P \approx \frac{1}{S\sqrt{4\langle I \rangle}} \tag{13}$$

and

$$\frac{\delta I^{\uparrow}}{I^{\uparrow}} \approx \frac{\delta P}{(1+P)}, \quad \frac{\delta I^{\downarrow}}{I^{\downarrow}} \approx \frac{\delta P}{(1-P)}, \tag{14}$$

with the assumption that the error in $I_{L,R}^{+,-}$ is simply $\sqrt{(I_{L,R}^{+,-})}$, as follows from the Poisson statistics of the photoelectron process.

III. RESULTS

With the present configuration the typical count rate on each quadrant of the anode for the iron "d" band emission is 15 000 Hz, at $h\nu = 60$ eV, normal emission, and with 800-mA stored beam current in the NSLS storage ring. The signal corresponds to an energy resolution of 0.35 eV. The optimum energy resolution with the present beamline is of the order of 0.1 eV. However, at this resolution with the configuration based on the miniature TGM, there are insufficient counts to perform spin analysis in a reasonable time scale. The angular resolution was approximately $\pm 1.5°$.

The sample magnetization is reversed on completion of each scan and successive even/odd ($\pm$) numbered scans are summed into separate channels. Consequently, four sets of data are collected from the left/right scattering channels ($I_L^+, I_R^+, I_L^-, I_R^-$) and another four from the up/down scattering channels, ($I_U^+, I_D^+, I_U^-, I_D^-$). The data acquisition system is able to display a running polarization spectrum generated using Eq. (9).

Figure 6 illustrates a data set obtained in approximately 20 min from a Fe(001) picture frame. These spectra are obtained at normal emission with $\theta_i = 35°$, corresponding to "s" polarized light. Figure 6(a) shows the instrumental asymmetry function as determined from Eq. (10). This provides a measure of the asymmetry independent of the actual polarization. There may be contributions to this function other than the imperfections in the relative sensitivity of the four quadrants and analyzer alignment: for example, a spin orbit generated polarization from the surface under study. An independent experimental measure of any spurious instrumental effects can be obtained by substituting a graphite target for the gold target. The graphite scattering target, being a low-Z material and hence having negligible spin-orbit effects, has an effective Sherman function of zero.

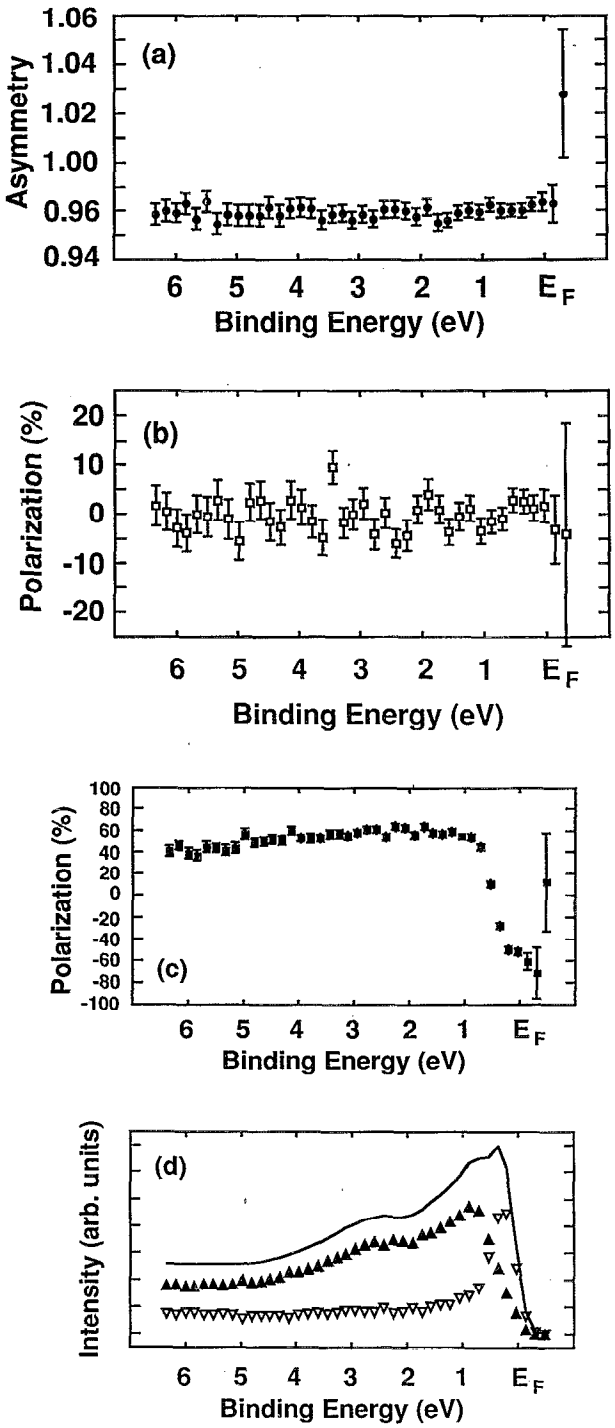

FIG. 6. Normal emission photoemission spectra from Fe(001) at $\theta_i = 35°$ and $h\nu = 60$ eV showing in (a) the instrumental asymmetry function [see Eq. (10)], (b) the polarization in the channel orthogonal to the magnetization direction, (c) the polarization Eq. (9) in the direction of the magnetization, and (d) the spin-resolved spectra [Eq. (11)], ▲▲▲▲ = majority, ▽▽▽▽ = minority and — = spin integrated.

As can be seen in Fig. 6(a), the instrumental asymmetry is relatively flat, with a slight offset from 1.0. Note that even if this function were strongly varying the polarization would not be affected. Figure 6(b) shows the measured

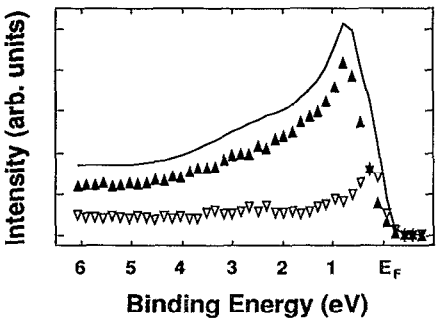

FIG. 7. Normal emission photoemission spectra from Fe(001) at $\theta_i = 70°$ and $h\nu = 60$ eV.

component of polarization in the direction orthogonal (i.e., up/down) to the sample magnetization direction. With this equal to zero, the analyzer and magnetization of the sample are well aligned. Figure 6(c) shows the measured polarization [Eq. (9)], and Fig. 6(d) the derived spin spectra [using Eq. (11)] together with the spin-integrated spectrum.

While Fig. 6 shows the spectra obtained with an angle of incidence for the light corresponding to s polarization, Fig. 7 shows the same sample for normal emission with $\theta_i = 70°$, or p-polarized light. Thus in these spectra bands of Δ_1 symmetry are highlighted over those of Δ_5 symmetry as observed in Fig. 6(d).

Finally Fig. 8 shows the spin-resolved spectra close to the surface zone boundary at $\overline{X}$ ($\sim 18°$ emission angle) and demonstrates the ability of the spectrometer to move off normal to measure the dispersion of spin-polarized electronic states. This capability has been extensively applied in the $p(1\times1)$ oxygen overlayer structure on Fe(001).[5(c)] Figures 6–8 thus illustrate the versatility of this instrument to perform full angle-resolved photoemission experiments with spin sensitivity.

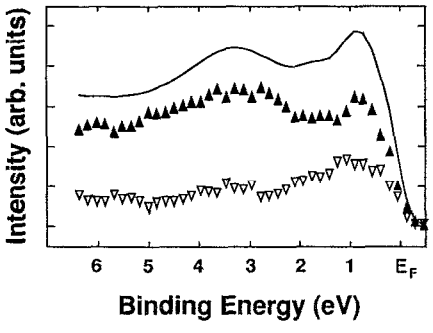

FIG. 8. Off-normal angle-resolved photoemission spectra from Fe(001). The angle of emission, $\theta_e = 18°$, $h\nu = 60$ eV, and $\theta_i = 35°$.

In summary, we have therefore demonstrated that the combination of two recent instrumental developments allows a previously difficult experiment to be performed with relative ease. The use of an undulator source more than compensates for the low efficiency of the spin detectors. At the same time the new compact low-energy spin detectors provide the flexibility required to perform angle and spin-resolved photoemission studies.

ACKNOWLEDGMENTS

We would like to express our thanks to the NSLS staff. This work was supported in part by U.S. Department of Energy Contract No. DE-AC02-76CH00016, the National Science Foundation Materials Research Group Contract No. DMR-86-03304, and by ONR.

[1] E. W. Plummer and W. Eberhardt, Adv. Chem. Phys. **49**, 533 (1982).
[2] M. Campagna, D. T. Pierce, F. Meier, K. Sattler, and H. C. Siegmann, Adv. Electron. Electron Phys. **41**, 113 (1976).
[3] E. Kisker, W. Gudat, E. Kuhlmann, R. Clauberg, and M. Campagna, Phys. Rev. Lett. **45**, 2053 (1980).
[4] E.g., E. Kisker, K. Schroder, W. Gudat, and M. Campagna, Phys. Rev. B **31**, 329 (1985) and R. Feder, Ed., *Polarized Electrons in Surface Physics* (World Scientific, Singapore, 1985), and references therein.
[5] (a) P. D. Johnson, A. Clarke, N. B. Brookes, S. L. Hulbert, B. Sinković, and N. V. Smith, Phys. Rev. Lett. **61**, 2257 (1988); (b) G. Schonhense, M. Getzlaff, C. Westphal, B. Heidemann, and J. Bansmann, J. Phys. (Paris) Colloq. **8**, C-1643 (1988); (c) A. Clarke, N. B. Brookes, P. D. Johnson, M. Weinert, B. Sinković, and N. V. Smith, Phys. Rev. B **41**, 9659 (1990).
[6] "Magnetism in Ultrathin Films," Special issue of Appl. Phys. A **49**, edited by D. Pescia (1989).
[7] D. T. Pierce, R. J. Celotta, M. H. Kelley, and J. Unguris, Nucl. Instrum. Methods A **266**, 550 (1988).
[8] J. Unguris, D. T. Pierce, and R. J. Celotta, Rev. Sci. Instrum. **57**, 1314 (1986).
[9] J. Kirschner and R. Feder, Phys. Rev. Lett. **42**, 1008 (1979).
[10] F. B. Dunning, L. G. Gray, J. M. Ratliff, F. -C. Tang, X. Zhang, and G. Walters, Rev. Sci. Instrum. **58**, 1706 (1987); F. -C. Tang, X. Zhang, F. B. Dunning, and G. K. Walters, *ibid.* **59**, 504 (1988).
[11] D. Tillmann, R. Thiel, and E. Kisker, Z. Phys. B **77**, 1 (1989).
[12] P. D. Johnson, J. Galayda, S. L. Hulbert, R. W. Klaffky, A. Luccio, G. Vignola, and C. Jacobsen, Nucl. Instrum. Methods A **266**, 106 (1988).
[13] S. Krinsky, M. L. Perlman, and R. E. Watson, *Handbook on Synchrotron Radiation*, edited by D. E. Eastman and Y. Farge (North-Holland, Amsterdam, 1983), Chap. 2.
[14] H. Bruck, *Accélérateurs Circulaires de Particules* (Presses Universitaires de France, 1966).
[15] W. R. McKinney and M. R. Howells, Nucl. Instrum. Methods **172**, 149 (1980).
[16] These expressions are only strictly valid for a mirror making a stigmatic focus.
[17] M. R. Howells, Nucl. Instrum. Methods **172**, 123 (1980).
[18] F. Cerrina, SPIE **503**, 68 (1984).
[19] S. Krinsky, IEEE Trans. Nucl. Sci. **NS-30**, 3078 (1983); K. -J. Kim, Nucl. Instrum. Methods A **246**, 71 (1986).
[20] HA50 Hemispherical Analyzer, VSW Ltd. Manchester, England.
[21] M. R. Scheinfein, D. T. Pierce, J. Unguris, J. J. McClelland, and R. J. Celotta, Rev. Sci. Instrum. **60**, 1 (1989).
[22] J. Kessler, *Polarized Electrons* (Springer, Berlin, 1976).